Research Article

Humaira Yasmin*, Safia Akram*, Maria Athar, Khalid Saeed, Alia Razia, and J. G. Al-Juaid

Impact of multiple slips on thermally radiative peristaltic transport of Sisko nanofluid with double diffusion convection, viscous dissipation, and induced magnetic field

https://doi.org/10.1515/ntrev-2024-0004
received November 20, 2023; accepted March 7, 2024

Abstract: The analysis focuses on investigating the phenomenon of double-diffusive convection using the Sisko nanofluid model. It particularly highlights the impact of induced magnetic flux, viscous dissipation, and heat radiation within an asymmetric geometry having multiple slip conditions. To ascertain the salient of the Brownian diffusion coefficient and thermophoresis, we have incorporated viscous dissipation, heat radiation, and the Buongiorno model. The Soret and Dufour parameters describe the convective double diffusion phenomenon. The mathematical formulation is constructed through equations governing magnetic force function, concentration, temperature, momentum, and continuity. These formulations yield nonlinear partial differential equations to explain the designated flow. To simplify the nonlinear partial differential equations, the lubrication paradigm of mathematical simulations is employed. The subsequent system of coupled nonlinear differential equations is calculated numerically through the NDSolve function, which is a built-in program of Mathematica. Numerical results and graphs give evidence that supports the significance of different flow quantities in physiological contexts. The findings from this investigation are anticipated to contribute to the development of intelligent magneto-peristaltic pumps, particularly in thermal and drug administration applications. The current investigation suggests that the distribution of temperature reduces as the coefficient of radiation increases due to a system's high heat emission and consequent effects of cooling. Furthermore, the increased influence of heat radiation raises the concentration profile. It is also highlighted that heat radiation has the potential to raise a fluid's temperature, which raises the volume fraction of nanoparticles.

Keywords: multiple slips, viscous dissipation, Sisko nanofluids, thermal radiation, double diffusion convection, asymmetric channel, induced magnetic field

*** Corresponding author: Humaira Yasmin,** Department of Basic Sciences, General Administration of the Preparatory Year, King Faisal University, P.O. Box 400, Al-Ahsa 31982, Saudi-Arabia; Department of Mathematics and Statistics, College of science, King Faisal University, P.O. Box 400, Al Ahsa 31982, Saudi-Arabia, e-mail: hhassain@kfu.edu.sa
*** Corresponding author: Safia Akram,** Department of Humanities and Basic Sciences, MCS, National University of Sciences and Technology, Islamabad, Pakistan, e-mail: drsafiaakram@gmail.com
Maria Athar: Department of Humanities and Sciences, SEECS, National University of Sciences and Technology, Islamabad, Pakistan
Khalid Saeed: School of Humanities and Sciences, College of Aeronautical Engineering, National University of Sciences and Technology, Islamabad, Pakistan
Alia Razia: Department of Humanities and Basic Sciences, MCS, National University of Sciences and Technology, Islamabad, Pakistan
J. G. Al-Juaid: Department of Mathematics and Statistics, College of Science, Taif University, P.O. Box 11099, Taif 21944, Saudi Arabia.

Nomenclature

c	propagation of velocity
C	solutal concentration
D_{B}	Brownian diffusion coefficient
D_{CT}	Soret diffusivity
D_{s}	solutal diffusivity
D_{T}	thermophoretic diffusion coefficient
D_{TC}	Dufour diffusivity
E	induced electric field
G_{rc}	solutal Grashof number
G_{rt}	thermal Grashof number
G_{rF}	nanoparticle Grashof number
g	acceleration due to gravity
J	current density
k	thermal conductivity
Le	Lewis number
Ln	nanofluid Lewis number
M	Hartmann number

N_b	Brownian motion parameter
N_{CT}	Soret parameter
N_t	thermophoresis parameter
N_{TC}	Dufour parameter
p	pressure
p_m	sum of ordinary and magnetic pressures
Pr	Prandtl number
Re	Reynolds number
R_m	magnetic Reynolds number
S_1	Stommer's number
T	temperature
t	time
U,V	velocities in X and Y directions
α_0, α_1	Sisko fluid parameters
ρ_f	fluid density
μ_e	magnetic permeability
ρ_{f_0}	fluid density at T_0
β_C	volumetric solutal expansion
ψ	stream function
σ	electrical conductivity
β_4, β_1	wave amplitudes
β_2, β_3	channel width
μ	fluid viscosity
ξ	magnetic diffusivity
Φ	magnetic force function
λ	wavelength
β_T	volumetric thermal expansion
$(\rho c)_p$	heat capacity of nanoparticle
γ	dimensionless solutal concentration
$(\rho c)_f$	heat capacity of fluid
δ	wave number
θ	dimensionless temperature
Ω	dimensionless nanoparticle volume fraction
Θ	nanoparticle volume fraction
ρ_p	nanoparticle mass density

1 Introduction

One of the significant physiological phenomena is peristaltic flow which has wide-ranging utilization in engineering fields and biomedicine, specifically in scenarios having micro/macro level transportation. These flows involve diverse functions both in human physiology and industrial applications that encompass transportation and excretion of body fluids as well as handling of corrosive liquids and various machine applications like roller and finger pumps. These diversified practical applications of peristaltic flow have instigated researchers to further explore the phenomenon. In 1960, Latham [1] explained this phenomenon in detail in his MS research where he explained the process as "natural siphon" which employs rhythmic squeezing that travels along the chamber walls and pushes the contents within the chamber or vessel. Jaffrin and Shapiro [2] conducted a detailed analysis of the process. Later, researchers like Misra and Rao [3], Hina *et al.* [4], Akbar *et al.* [5], Safia Akram *et al.* [6], and Nadeem *et al.* [7–10] experimented with the process having different fluids under various conditions involving numerous parameters both physiological and mechanical. Despite these investigations, there are diverse limitations and unresolved issues which necessitate further in-depth analysis and exploration.

Another influential area of peristaltic flow is nanofluids which have significant applications in medical engineering and biomedicine. The composition of nanofluid contains tiny oxides of metals, carbon nanotubes, and other carbon ions. However, the quantity of nanoparticles is minimal, which is calculated as less than 5%. Incredibly, a negligible amount like 1% added in the base fluid of nanostructure like fibre, sheet, rod, or wire could augment the heat properties by a considerable increase in heat conductivity. So, the addition of a minimal amount of nanoparticles can significantly enhance thermal flow. Choi and Eastman [11] explained the dispersion of nanosized particles within a heat-transmitting fluid. Similarly, Masuda *et al.* [12] further explored the nanofluid properties in terms of heat expansion and conductivity. A model is devised by Duangthongsuk and Wongwises [13] to examine nanofluid's thermophysical characteristics and its impact on the liquid's convection heat flow constant at the lowest nanoparticle concentration. Buongiorno and Hu [14] and Buongiorno [15] have investigated the Brownian diffusion with thermophoresis to understand the convective flow in nanofluids by applying a closed-form model. Another development to explain the dispersion of concentration polarity within the range of micro to nanochannel is through various models of analysis that is done by Mani *et al.* [16]. Whereas Akbar and Nadeem [17] combined the concept of nanofluids with models of peristaltic pumping to examine the nanofluid peristaltic flow under the endoscopic influence. Moreover, Akbar [18] observed the Sisko nanoliquid peristaltic flow in an asymmetric channel. Particularly, the examination reveals that an increase in parameter axial pressure of Sisko nanoliquid leads to a rise in the area of peristaltic pumping. The research literature contains a wide range of studies [19–25] which further shed light on the phenomena of non-Newtonian and Newtonian nanofluids under various parameters and different flow structures. Moreover, the concept of magnetohydrodynamics is salient in sweltering heat equipment like electric transformers, as well as in corporal conductive matter including pumps and machines for blood regulation and

arterial blood flow, Magnetic resonance imaging, equipment for magnetic therapies, and in aviation where inclined magnetic flux impact is noticeable. In biomedicine and medical engineering issues, [26–30] peristaltic flow with magnetic flux has provided multifaceted solutions. In electrically charged fluids having optimal Reynolds number, magnetic diffusion is negligible as compared to induction, hence resulting in the significant impact of induced magnetic flux. Taking into consideration the velocity slip conditions, Shit *et al.* [31] observed the micropolar fluid peristalsis under magnetic flux. The results reveal the strengthening of peristalsis flow under magnetic influence causing mechanical simulation of the fluid. Therefore, induced magnetic force is effective for the treatment of cancers and magneto therapy is recommended in research [32–34]. Other notable findings are given in previous studies [29,35–39].

The study of hydromagnetic peristaltic flow under thermal production and consumption impact has significant importance in various engineering and scientific fields. These encompass multifarious applications like processing of energy, and cooling and heating systems employed in industrial processing and in space technology and devices. Additional research exploring the phenomenon of peristalsis with heat and nanofluids is referred in previous studies [40–44]. These investigations further delved into the various parameters including Brownian conditions, Hartmann number, and thermophoresis.

Double diffusion is a phenomenon of typology of convection with two asymmetric density gradients called solutal and density gradients, respectively. It exhibits differing diffusion rates. Numerous natural, technical, and industrial scenarios use blended convection motion that integrates the force and free convection flows. Any fluid having two contrasting density gradients at differing rate of diffusion leads to free mixed convection with double diffusion [45,46]. The practical utilization of hydromagnetic flow with heat dissemination properties includes wide industrial applications in nuclear reactor processes, manufacturing of electronic equipment and devices, which are few to mention. Owing to its extensive scope, the phenomenon has been investigated with various models of peristalsis and nanofluids flow [47–53].

Furthermore, the conventional use of no-slip situation is inefficient in case of fluids having wall slip condition with macroscopic context as it involves the relation of grip and slip velocity. The role of slip condition is salient in different procedures such as hysteresis impacts, spurt, and shear skin. Similarly, nanofluids with boundary slip conditions are used in technology to build devices like artificial heart valves and conduits. Further notable studies are referred in previous studies [54–59].

Due to the vast applications of the phenomenon mentioned above, the present study employs a unique merging of various intricate factors like heat radiation, induced magnetic flux, peristaltic transportation, viscous dissolution, multiple slip conditions, nanofluid, and double diffusive convection. The aim of the current investigation is to analyse the flow behaviour employing advanced mathematical and computational techniques. The study focuses on the fluid transportation with 2D peristalsis in an asymmetric channel. The driving force of the flow is sinusoidal waves transmitted through walls of the chamber with specific wavelength and persistent speed. The equation of temperature, mass, magnetic flux, concentration, momentum, and nanoparticle fraction is employed on fluid peristaltic transportation across the channel walls under slip boundary conditions. For the study, Mathematica command, NDSolve is employed for numerical solutions along with non-dimensional procedure. The result's findings are represented in graphical representations of concentration, velocity, nanoparticle fraction, magnetic force function, and temperature that not only provides ease in the analysis but also depicts parameters variation and its impact on system's behaviour. A comprehensive analysis of the results findings is presented in Section 4, while the significant resultant factors are summed up in the conclusion. It is noteworthy that insight of the convective double diffusion phenomenon upon nanoparticles in peristalsis have significance to assist in boosting nanofluid devices, enhance devices using microfluids, efficacious drug delivery, and proficient heat transmission systems.

2 Mathematical model

To investigate the peristaltic flow of Sisko nanofluid under dense and electrically charged medium, we consider the analysis of a two-dimensional channel, characterized by width $\beta_3 + \beta_2$. The channel promotes sinusoidal waves at uniform velocity along the channel walls, serving as the source of initial flow. To facilitate the study, a coordinates system is adopted where the centre of the channel is aligned with X-axis, while the cross section of the channel lies along the Y-axis. The geometry of the problem under consideration is given in Figure 1.

The mathematical depiction of the wall's geometric forms is described as follows:

$$\begin{aligned} Y = W_1 &= \beta_3 + \beta_4 \cos\left[\frac{2\pi}{\lambda}(X - ct)\right], \\ Y = W_2 &= -\beta_2 - \beta_1 \cos\left[\frac{2\pi}{\lambda}(X - ct) + \varphi\right], \end{aligned} \tag{1}$$

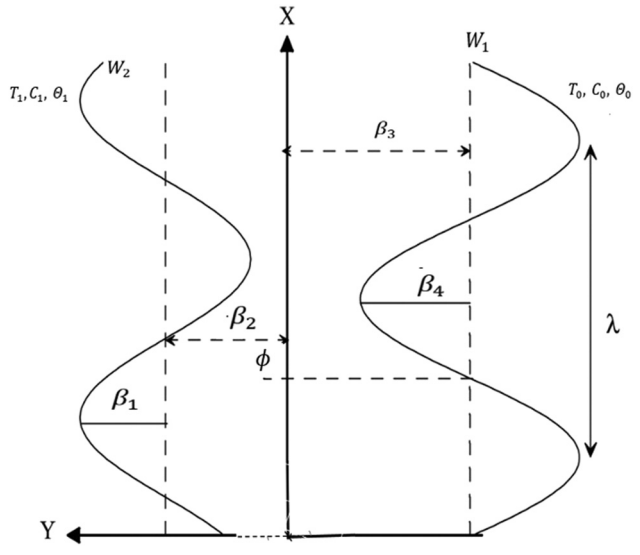

Figure 1: Geometry of the problem.

where $\beta_3 + \beta_2$ indicates the channel width, (β_4, β_1) stands for the wave amplitudes, c represents the speed of velocity, λ refers to the wavelength, and the time is represented by t. The phase difference is represented by φ having a range of $0 \le \varphi \le \pi$. Moreover, when $\varphi = 0$, it represents a symmetric channel with no phase wave, and when $\varphi = \pi$ it represents a channel with a phase wave. Also β_1, β_2, β_3, β_4, and φ satisfy the condition $\beta_4^2 + \beta_1^2 + 2\beta_4\beta_1 \cos\varphi \le (\beta_3 + \beta_2)^2$.

In this analysis, the right ($y = W_1$) and left ($y = W_2$) walls are retained at temperature (T_0, T_1), concentration of the solvent at (C_0, C_1), and nanoparticles volume fraction (Θ_0, Θ_1). The velocity $V = (U(X, Y, t), V(X, Y, t), 0)$ is used to represent the flow as two-dimensional and directional. Additionally, we introduced an outer transverse magnetic flux at uniform rate Z_0, an induced magnetic force $Z(z_X(X, Y, t), z_Y(X, Y, t), 0)$ and accumulative magnetic flux $Z^+(z_X(X, Y, t), Z_0 + z_Y(X, Y, t), 0)$ for the analysis.

The basic equations for hydro-magnetic Sisko nanofluid are as follows:

(a) Maxwell's equation [31–33] is given as

$$\nabla \cdot \boldsymbol{E} = 0, \quad \nabla \cdot \boldsymbol{Z} = 0, \tag{2}$$

$$\nabla \times \boldsymbol{Z} = \boldsymbol{J}, \mathbf{J} = \sigma\{\mathrm{E} + \mu_e(\boldsymbol{V} \times \boldsymbol{Z}^+)\}, \tag{3}$$

$$\nabla \times \boldsymbol{E} = -\mu_e \frac{\partial \boldsymbol{Z}}{\partial t}, \tag{4}$$

where V, E, μ_e, J, and σ refer to the velocity vector, induced electric field, magnetic permeability, current density, and electric conductivity.

(b) Equation of continuity is given as

$$\nabla \cdot \boldsymbol{V} = 0. \tag{5}$$

(c) Momentum equation is defined as [47,48,50]

$$\begin{aligned} \rho\left(\frac{\mathrm{d}\boldsymbol{V}}{\mathrm{d}t}\right) &= \nabla \cdot \tau - \mu_e(\boldsymbol{Z}^+ \cdot \nabla)\boldsymbol{Z}^+ - \nabla\left(\frac{1}{2}\mu_e(\boldsymbol{Z}^+)^2\right) \\ &+ g\{\rho_{f0}(1 - \Theta_0)\{\beta_T(T - T_0) + (C - C_0)\beta_C\} \\ &-(\rho_p - \rho_{f0})(\Theta - \Theta_0)\}, \end{aligned} \tag{6}$$

where T indicates the temperature, $\frac{\mathrm{d}}{\mathrm{d}t}$ is the material derivative, g stands for the acceleration, ρ_{f0} indicates the fluid density at T_0, β_T refers to the coefficient of volumetric thermal expansion, β_C stands for the coefficient of volumetric solutal expansion, ρ_p represents the mass density of nanoparticle, C refers to the concentration, Θ stands for the nanoparticle volume fraction, τ is the stress tensor for the Sisko fluid which is a kind of viscoelastic fluid that possesses both elastic and viscous features. The mathematical form of Sisko fluid stress tensor is defined as [7,18]

$$\tau = -P\boldsymbol{I} + \boldsymbol{S}, \tag{7}$$

$$\begin{aligned} S &= (\alpha_0 + \alpha_1(\sqrt{\boldsymbol{\Pi}})^{i-1})A_1, \quad A_1 = L + L^T \\ L &= \mathrm{grad}\,\boldsymbol{V}, \Pi = \frac{1}{2}\mathrm{trac}(A_1^2), \end{aligned} \tag{8}$$

where P stands for the pressure and I is the Identity tensor.

(d) The nanoparticle thermal energy equation in the presence of mixed convection, radioactive heat flux, and viscous dissipation is defined as [49,52]

$$\begin{aligned} (\rho c)_f\left(\frac{\mathrm{d}T}{\mathrm{d}t}\right) &= k\nabla^2 T + (\rho c)_p\left[D_B(\nabla\boldsymbol{\Theta} \cdot \nabla\boldsymbol{T}) + \left(\frac{D_T}{T_0}\right)\nabla^2 T\right] \\ &+ \boldsymbol{S} \cdot \boldsymbol{L} - \nabla q_r + D_{TC}\nabla^2 C, \end{aligned} \tag{9}$$

where $(\rho c)_f$ refers to the fluid's heat capacity, k stands for the thermal conductivity, $(\rho c)_p$ represents the heat capacity of effective nanoparticles, D_B is the component of Brownian diffusion, D_T refers to the coefficient of thermophoretic diffusion, D_{TC} stands for the Dufour diffusivity, L stands for the velocity gradient, ∇^2 stands for the Laplacian operator, and q_r stands for the radiation thermal flux, which can be established by using the Rosseland diffusion technique as:

$$q_r = -\frac{4\sigma^*}{3k^*}\frac{\partial T^4}{\partial Y}. \tag{10}$$

The tremendous radiation limit is considered in this investigation. Therefore, by assuming that there are not any substantial temperature changes inside the flow channel, Taylor expansion may be used to modify T^4 such that temperature can be expressed as a linear function. With respect to T_0, Taylor expansion on T^4 is now defined as

$$T^4 = T_0^4 + 4T_0^3(T - T_0) + 6T_0^2(T - T_0)^2 + ... \tag{11}$$

Now we obtain $(T - T_0)$ by omitting the higher powers of T (more than the first).

$$T^4 = 4T_0^3T - 3T_0^4. \tag{12}$$

Eqs. (11) and (12) yield

$$q_r = -\frac{16\sigma^*T_0^3}{3k^*}\frac{\partial T}{\partial Y}, \tag{13}$$

$$\frac{\partial q_r}{\partial Y} = -\frac{16\sigma^*T_0^3}{3k^*}\frac{\partial^2 T}{\partial Y^2}, \tag{14}$$

where k^* is the Rosseland mean absorption and σ^* represents the Stefan–Boltzmann constant.

(e) The solute concentration is defined as [49,52]

$$\frac{\mathrm{d}C}{\mathrm{d}t} = D_s\nabla^2 C + D_{CT}\nabla^2 T, \tag{15}$$

where D_{CT} and D_{s} indicate Soret diffusivity and solutal diffusivity, respectively.

(f) The nanoparticle volume fraction is defined as [49,52]

$$\frac{\mathrm{d}\Theta}{\mathrm{d}t} = D_{\mathrm{B}}\nabla^2\Theta + \left(\frac{D_{\mathrm{T}}}{T_0}\right)\nabla^2 T. \tag{16}$$

(g) The induction equation is calculated by means of equations (2)–(4)

$$\frac{\partial \boldsymbol{Z}^+}{\partial t} = \nabla\times(\boldsymbol{V}\times\boldsymbol{Z}^+) + \frac{1}{\xi}\nabla^2\boldsymbol{Z}^+, \tag{17}$$

where $\xi = \mu_{\mathrm{e}}\sigma$ is magnetic diffusivity.

Since we are interested in performing the flow simulation in wave frame (x, y). Therefore, the Galilean transformation relates the velocities and coordinates in the laboratory (X, Y) and wave (x, y) frames as

$$\begin{aligned} &u = U - c, y = Y, x = X - ct, p(x, y) = P(X, Y, t),\\ &v = V, \end{aligned} \tag{18}$$

where (u, v) and (U, V) indicate the velocities in wave and laboratory frames, respectively.

The following quantities are defined in order to express the flow of fluid in a non-dimensional form as

$$\begin{aligned}
&\bar{x} = \frac{x}{\lambda}, m_1 = \frac{\beta_4}{\beta_3}, \bar{y} = \frac{y}{\beta_3}, \delta = \frac{\beta_3}{\lambda}, \bar{u} = \frac{u}{c}, m = \frac{\beta_2}{\beta_3},\\
&\bar{t} = \frac{ct}{\lambda}, w_2 = \frac{W_2}{\beta_2}, w_1 = \frac{W_1}{\beta_3}, m_0 = \frac{\beta_1}{\beta_3}, \bar{p} = \frac{\beta_3^2 p}{\mu c\lambda},\\
&\mathrm{Pr} = \frac{(\rho c)_{\mathrm{f}}\ \upsilon}{k}, \mathrm{Re} = \frac{\rho_{\mathrm{f}} c\beta_3}{\mu}, \upsilon = \frac{\mu}{\rho_{\mathrm{f}}}, \mathrm{Le} = \frac{\upsilon}{D_{\mathrm{s}}},\\
&\mathrm{Ln} = \frac{\upsilon}{D_{\mathrm{B}}}, \theta = \frac{T - T_0}{T_1 - T_0}, \bar{\nu} = \frac{\nu}{c}, \gamma = \frac{C - C_0}{C_1 - C_0},\\
&\Omega = \frac{\Theta - \Theta_0}{\Theta_1 - \Theta_0}, \bar{S}_{xx} = \frac{S_{xx}\lambda}{\mu c}, \bar{S}_{xy} = \frac{S_{xy}\beta_3}{\mu c},\\
&\bar{S}_{yy} = \frac{S_{yy}\beta_3}{\mu c}, N_{CT} = \frac{D_{\mathrm{CT}}(T_1 - T_0)}{D_{\mathrm{s}}(C_1 - C_0)},\\
&N_{\mathrm{b}} = \frac{(\rho c)_{\mathrm{p}} D_{\mathrm{B}}(\Theta_1 - \Theta_0)}{k},\\
&G_{\mathrm{rc}} = \frac{g(1 - \Theta_0)\rho_{\mathrm{f}}\beta_{\mathrm{c}}(C_1 - C_0)\beta_3^2}{\mu c},\\
&N_{\mathrm{TC}} = \frac{D_{\mathrm{CT}}(C_1 - C_0)}{k(T_1 - T_0)},\\
&G_{\mathrm{rt}} = \frac{g\beta_3^2(1 - \Theta_0)(T_1 - T_0)\rho_{\mathrm{f}}\beta_{\mathrm{T}}}{\mu c},\\
&\mathrm{Rd} = -\frac{16\sigma^*T_1^3}{3k^*}, G_{\mathrm{rF}} = \frac{g(\rho_{\mathrm{p}} - \rho_{\mathrm{f}})(\Theta_1 - \Theta_0)\beta_3^2}{\mu c},\\
&N_{\mathrm{t}} = \frac{(\rho c)_{\mathrm{p}} D_{\mathrm{T}}(T_1 - T_0)}{T_0 k}, u = \frac{\partial\psi}{\partial y}, h_{\mathrm{x}} = \frac{\partial\Phi}{\partial y}, \mathrm{Br} = \mathrm{EcPr},\\
&v = -\delta\frac{\partial\psi}{\partial x}, r = \frac{\alpha_1}{\alpha_0(\beta_3/c)^{i-1}}, M = \sqrt{\frac{\sigma}{\mu}}B_0\beta_3,\\
&R_{\mathrm{m}} = \sigma c\beta_3\mu_{\mathrm{e}}, \bar{\Phi} = \frac{\Phi}{Z_0\beta_3}, h_{\mathrm{y}} = -\delta\frac{\partial\Phi}{\partial x}.
\end{aligned} \tag{19}$$

Using Eqs. (18) and (19), Eq. (5) is automatically satisfied and Eqs. (6)–(17) in terms of the stream function ψ and magnetic force function Φ (dropping the bars) are as follows:

$$\begin{aligned}
&\mathrm{Re}\delta(\psi_y\psi_{xy} - \psi_x\psi_{yy})\\
&\quad = -\frac{\partial p_{\mathrm{m}}}{\partial x} + \delta^2\frac{\partial S_{xx}}{\partial x} + \frac{\partial S_{xy}}{\partial y} + \mathrm{Re}S_1^2\Phi_{yy}\\
&\qquad + \mathrm{Re}S_1^2\delta(\Phi_y\Phi_{xy} - \Phi_x\Phi_{yy}) + G_{\mathrm{rt}}\theta + G_{\mathrm{rc}}\gamma - G_{\mathrm{rF}}\Omega,
\end{aligned} \tag{20}$$

$$\begin{aligned}
&\mathrm{Re}\delta^3(\psi_x\psi_{xy} - \psi_y\psi_{xx})\\
&\quad = -\frac{\partial p_{\mathrm{m}}}{\partial y} + \delta^2\frac{\partial S_{xy}}{\partial x} + \delta\frac{\partial S_{yy}}{\partial y} - \mathrm{Re}\delta^2S_1^2\Phi_{yy},\\
&\qquad - \mathrm{Re}S_1^2\delta^3(\Phi_y\Phi_{xx} - \Phi_x\Phi_{xy})
\end{aligned} \tag{21}$$

$$\begin{aligned}
\mathrm{Re}(\psi_y\theta_x - \psi_x\theta_y) &= \frac{1}{\mathrm{Pr}}(\theta_{yy} + \delta^2\theta_{xx}) + N_{\mathrm{TC}}(\delta^2\gamma_{xx} + \gamma_{yy})\\
&\quad + \mathrm{Rd}\theta_{yy} + N_{\mathrm{b}}(\delta^2\Omega_x\theta_x + \theta_y\Omega_y)\\
&\quad + \mathrm{Ec}(\delta^2S_{xx}\psi_{xy} + S_{xy}(\psi_{yy} - \delta^2\psi_{xx})\\
&\quad - \delta S_{yy}\psi_{xy}) + N_{\mathrm{t}}((\theta_y)^2 + \delta^2(\theta_x)^2),
\end{aligned} \tag{22}$$

$$\begin{aligned}&\mathrm{Re}\,\delta\mathrm{Le}(\psi_y\gamma_x - \psi_x\gamma_y)\\&\quad = (\gamma_{yy} + \delta^2\gamma_{xx}) + N_{\mathrm{CT}}(\theta_{yy} + \delta^2\theta_{xx})\end{aligned}, \tag{23}$$

$$\begin{aligned}&\mathrm{Re}\,\delta\mathrm{Ln}(\Omega_x\psi_y - \Omega_y\psi_x)\\&\quad = (\Omega_{yy} + \delta^2\Omega_{xx}) + \frac{N_{\mathrm{t}}}{N_{\mathrm{b}}}(\delta^2\theta_{xx} + \theta_{yy})\end{aligned}, \tag{24}$$

$$\psi_y - \delta(\Phi_x\psi_y - \Phi_y\psi_x) + \frac{1}{R_{\mathrm{m}}}(\delta^2\Phi_{xx} + \Phi_{yy}) = E, \tag{25}$$

where N_{CT} illustrates the Soret parameter, Ω represents the nanoparticle fraction, N_{t} stands for the thermophoresis parameters, δ symbolizes the wave number, Ln represents the nanofluid Lewis number, G_{rF} stands for the nanoparticle Grashof number, Re refers to the Reynolds number, Le stands for the Lewis number, N_{TC} stands for the Dufour parameter, N_{b} represents the Brownian motion, γ represents the solutal (species) concentration, G_{rt} stands for the thermal Grashof number, θ represents the temperature, G_{rc} stands for the solutal Grashof number, Pr is the Prandtl number, R_{m} is the magnetic Reynolds number, and (S_{xx}, S_{xy}, S_{yy}) are the non-dimensional form of stresses determined from equation (8), and is defined as follows:

$$S_{xx} = 2\delta\left(1 + r\left\{2\delta^2\left(\frac{\partial^2\psi}{\partial x\partial y}\right)^2 + \left(\frac{\partial^2\psi}{\partial y^2} - \delta^2\frac{\partial^2\psi}{\partial x^2}\right)^2 + 2\delta^2\left(\frac{\partial^2\psi}{\partial x\partial y}\right)^2\right\}^{\frac{i-1}{2}}\right)\frac{\partial^2\psi}{\partial x\partial y},$$

$$\begin{aligned}S_{xy} &= \left(1 + r\left\{2\delta^2\left(\frac{\partial^2\psi}{\partial x\partial y}\right)^2 + \left(\frac{\partial^2\psi}{\partial y^2} - \delta^2\frac{\partial^2\psi}{\partial x^2}\right)^2 + 2\delta^2\left(\frac{\partial^2\psi}{\partial x\partial y}\right)^2\right\}^{\frac{i-1}{2}}\right)\left(\frac{\partial^2\psi}{\partial y^2}\right.\\&\quad \left. - \delta^2\frac{\partial^2\psi}{\partial x^2}\right), S_{yy}\\&= -2\delta\left(1 + r\left\{2\delta^2\left(\frac{\partial^2\psi}{\partial x\partial y}\right)^2 + \left(\frac{\partial^2\psi}{\partial y^2} - \delta^2\frac{\partial^2\psi}{\partial x^2}\right)^2 + 2\delta^2\left(\frac{\partial^2\psi}{\partial x\partial y}\right)^2\right\}^{\frac{i-1}{2}}\right)\frac{\partial^2\psi}{\partial x\partial y}.\end{aligned}$$

Now using $\delta \ll 1$ (long wavelength) and finite approximation of a low Reynolds number, Eqs. (20)–(26) become

$$\frac{\partial p}{\partial x} = \frac{\partial}{\partial y}S_{xy} + \mathrm{Re}S_1^2\Phi_{yy} + G_{\mathrm{rt}}\theta + G_{\mathrm{rc}}\gamma - G_{\mathrm{rF}}\Omega, \tag{27}$$

$$0 = -\frac{\partial p}{\partial y}, \tag{28}$$

$$\begin{aligned}0 = \frac{\partial^2\theta}{\partial y^2} &+ N_{\mathrm{TC}}\mathrm{Pr}\frac{\partial^2\gamma}{\partial y^2} + N_{\mathrm{b}}\mathrm{Pr}\left(\frac{\partial\theta}{\partial y}\frac{\partial\Omega}{\partial y}\right) + N_{\mathrm{t}}\mathrm{Pr}\left(\frac{\partial\theta}{\partial y}\right)^2\\&+ \mathrm{RdPr}\frac{\partial^2\theta}{\partial y^2} + \mathrm{Br}\left(\frac{\partial^2\psi}{\partial y^2}\right)\left[\frac{\partial^2\psi}{\partial y^2} + r\left(\frac{\partial^2\psi}{\partial y^2}\right)^i\right],\end{aligned} \tag{29}$$

$$\frac{\partial^2\gamma}{\partial y^2} + N_{\mathrm{CT}}\frac{\partial^2\theta}{\partial y^2} = 0, \tag{30}$$

$$\frac{\partial^2\Omega}{\partial y^2} + \frac{N_{\mathrm{t}}}{N_{\mathrm{b}}}\frac{\partial^2\theta}{\partial y^2} = 0, \tag{31}$$

$$\Phi_{yy} = R_{\mathrm{m}}\left(E - \frac{\partial\psi}{\partial y}\right), \tag{32}$$

where

$$S_{xy} = \left(1 + r\left\{\left(\frac{\partial^2\psi}{\partial y^2}\right)^2\right\}^{\frac{i-1}{2}}\right)\frac{\partial^2\psi}{\partial y^2}. \tag{33}$$

Now pressure is eliminated from Eqs. (27) and (28) to yield the stream function equation as

$$\begin{aligned}&\frac{\partial^2}{\partial y^2}\left[\left(1 + r\left\{\left(\frac{\partial^2\psi}{\partial y^2}\right)^2\right\}^{\frac{i-1}{2}}\right)\frac{\partial^2\psi}{\partial y^2}\right] - \mathrm{Re}S_1^2R_{\mathrm{m}}\frac{\partial^2\psi}{\partial y^2} + G_{\mathrm{rt}}\frac{\partial\theta}{\partial y}\\&\quad + G_{\mathrm{rc}}\frac{\partial\gamma}{\partial y} - G_{\mathrm{rF}}\frac{\partial\Omega}{\partial y} = 0.\end{aligned} \tag{34}$$

The boundary conditions in non-dimensional form are expressed as

$$\begin{aligned}\psi &= \frac{F}{2}, \quad \frac{\partial\psi}{\partial y} = -l_1S_{xy} - 1 \text{ on } y = w_1(x),\\ \psi &= -\frac{F}{2}, \quad \frac{\partial\psi}{\partial y} = l_1S_{xy} - 1 \text{ on } y = w_2(x),\end{aligned} \tag{35}$$

$$\theta + l_2\frac{\partial\theta}{\partial y} = 0, \text{ on } y = w_1, \theta - l_2\frac{\partial\theta}{\partial y} = 1, \text{ on } y = w_2, \tag{36}$$

$$\gamma + l_3\frac{\partial\gamma}{\partial y} = 0, \text{ on } y = w_1, \gamma - l_3\frac{\partial\gamma}{\partial y} = 1, \text{ on } y = w_2, \tag{37}$$

$$\Omega + l_4\frac{\partial\Omega}{\partial y} = 0, \text{ on } y = w_1, \Omega - l_4\frac{\partial\Omega}{\partial y} = 1, \text{ on } y = w_2, \tag{38}$$

$$\Phi = 0, \text{ at } y = w_1(x) \text{ and } y = w_2(x), \tag{39}$$

where l_1, l_2, l_3, and l_4 stands for velocity slip parameter, temperature slip parameter, concentration slip parameter, and nanoparticle slip parameter, respectively. The no slip conditions in the aforementioned criteria are indicated when $l_1, l_2, l_3, l_4 = 0$.

The mean flow (Q) in non-dimensional form is computed as

$$Q = 1 + m + F, \tag{40}$$

where

$$F = \int_{w_2(x)}^{w_1(x)}\frac{\partial\psi}{\partial y}\mathrm{d}y = \psi(w_1(x)) - \psi(w_2(x)), \tag{41}$$

where

Table 1: Comparison of the current problem with available literature

Profile of velocity (u)				
$y = h(x)$	Current problem	Akbar [18]	Mehmood *et al.* [55]	Viscous fluid [3]
1.6472	−0.000806	−1	−0.0179032	−1
1.23979	0.282405	−0.317149	0.262324	−0.168407
0.83237	0.511743	0.309694	0.500021	0.478388
0.424954	0.674745	0.863047	0.686395	0.940385
0.0175371	0.769948	1.31172	0.808947	1.21758
−0.38988	0.802025	1.57029	0.852524	1.30998
−0.797296	0.774457	1.40441	0.808946	1.21758
−1.20471	0.685145	0.976262	0.686394	0.940385
−1.61213	0.529514	0.411789	0.50002	0.478388
−2.01955	0.306978	−0.252917	0.262323	−0.168407
−2.42696	0.024901	−1	−0.0179043	1

$$w_1(x) = 1 + m_1 \cos 2\pi x, \quad w_2(x) = -m - m_0 \cos(2\pi x + \varphi). \tag{42}$$

3 Special cases

- The results of Akbar [18] can be recovered as a special case of our problem by dropping/ignoring the phenomena of induced magnetic field (Φ), viscous dissipation (Br), slip parameters (l_1, l_2, l_3, l_4), thermal radiation (Rd), solutal (species) concentration (γ).
- The outcomes of Mehmood *et al.* [55] may be obtained as a special case of our problem by dropping the phenomena of double diffusion convection (G_{rF}, G_{rt}, G_{rc}), induced magnetic field (Φ), thermal radiation (Rd), solutal (species)

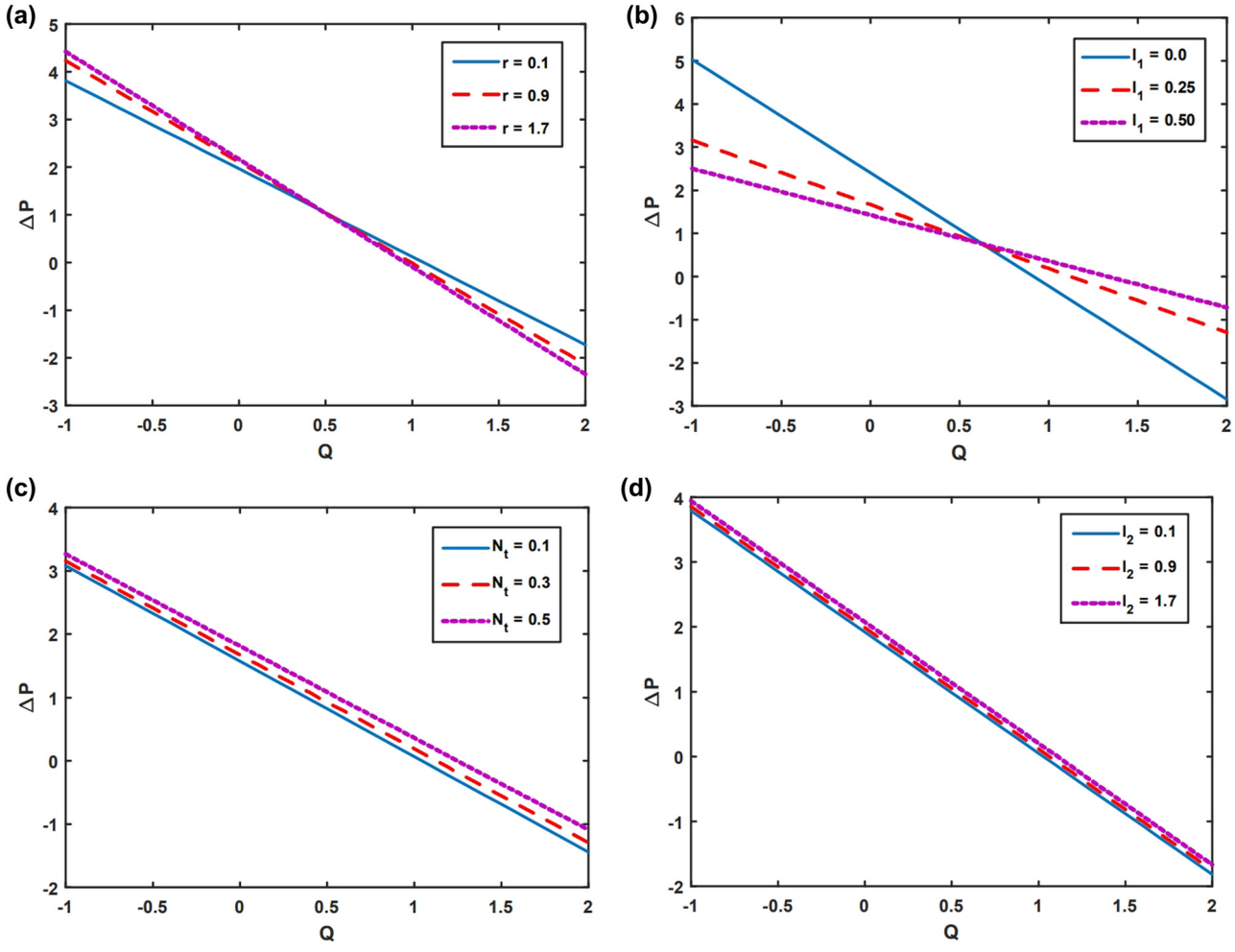

Figure 2: Behaviour of Pressure rise on r, l_1, N_t, and l_2.

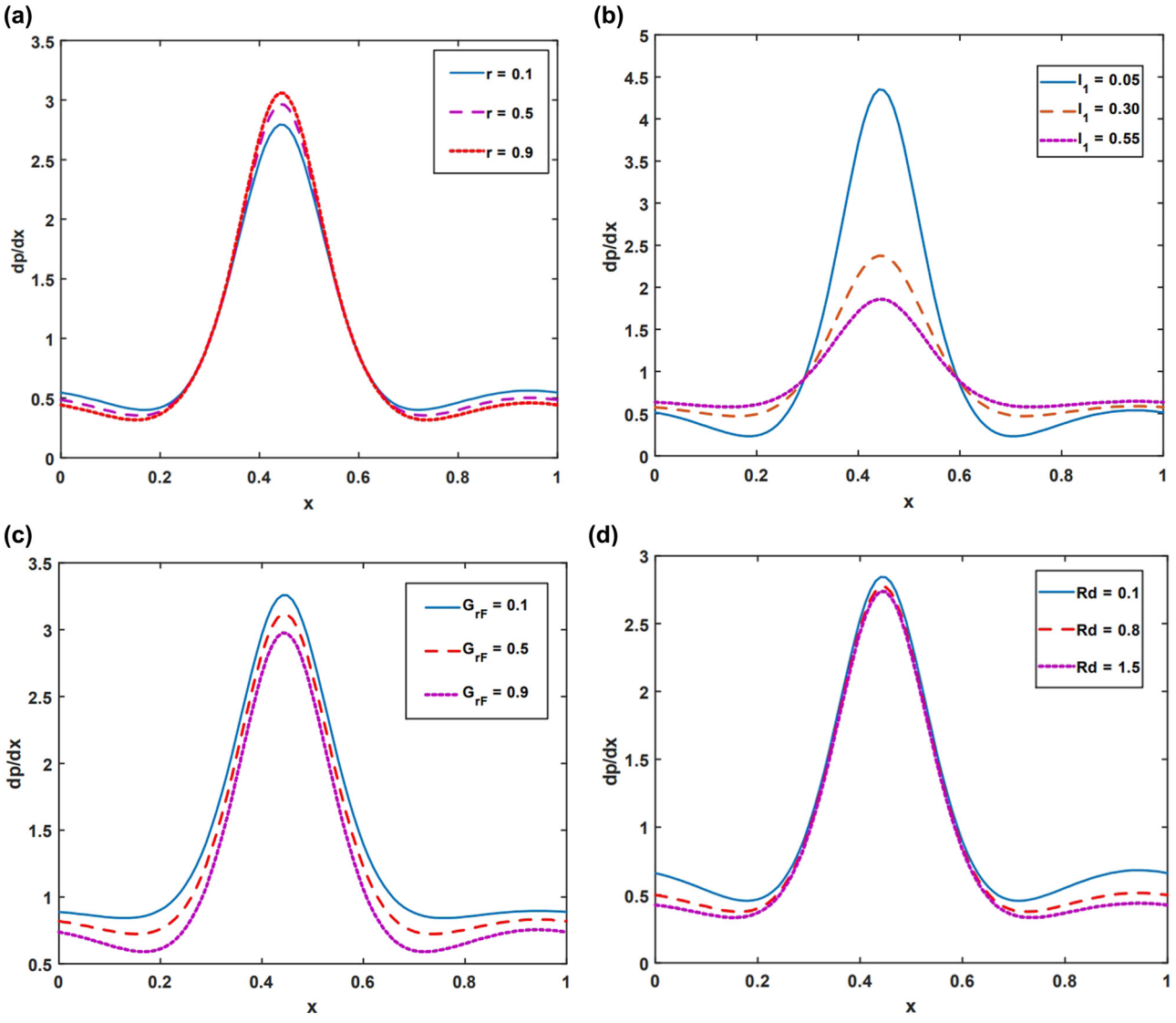

Figure 3: Pressure gradient impact on r, l_1, G_{rF}, and Rd.

concentration (γ), nanoparticle fraction (Ω), and slip parameters (l_3, l_4).

- By considering the value of the non-Newtonian parameter (r) = 0 and excluding the phenomena of heat transfer, double diffusion convection, slip parameters, and induced magnetic field, the results of the viscous fluid [3] can be found as a special case of our problem (Table 1).

4 Numerical solution and graphical analysis

The exact solution to Eqs. (27), (29)–(32), and (34) appears to be difficult to attain; the solution may be found by using computing techniques. Mathematica 9 and MATLAB software is used for performing the numerical computations of Eqs. (27), (29)–(32), and (34). NDSolve command is utilized for solving the nonlinear equations in Mathematica. NDSolve is basically a Wolfram Language function that is used to solve numerical differential equations. It is capable of solving a large variety of ordinary differential equations and certain partial differential equations. In NDSolve, the solutions for the functions are represented by interpolating function objects. The interpolating function objects approximate the function throughout the independent variable's range of minimum to maximum values. In general, NDSolve iteratively discovers solutions. To investigate the thermodynamic features of our model, a graphical analysis of the numerical results is produced.

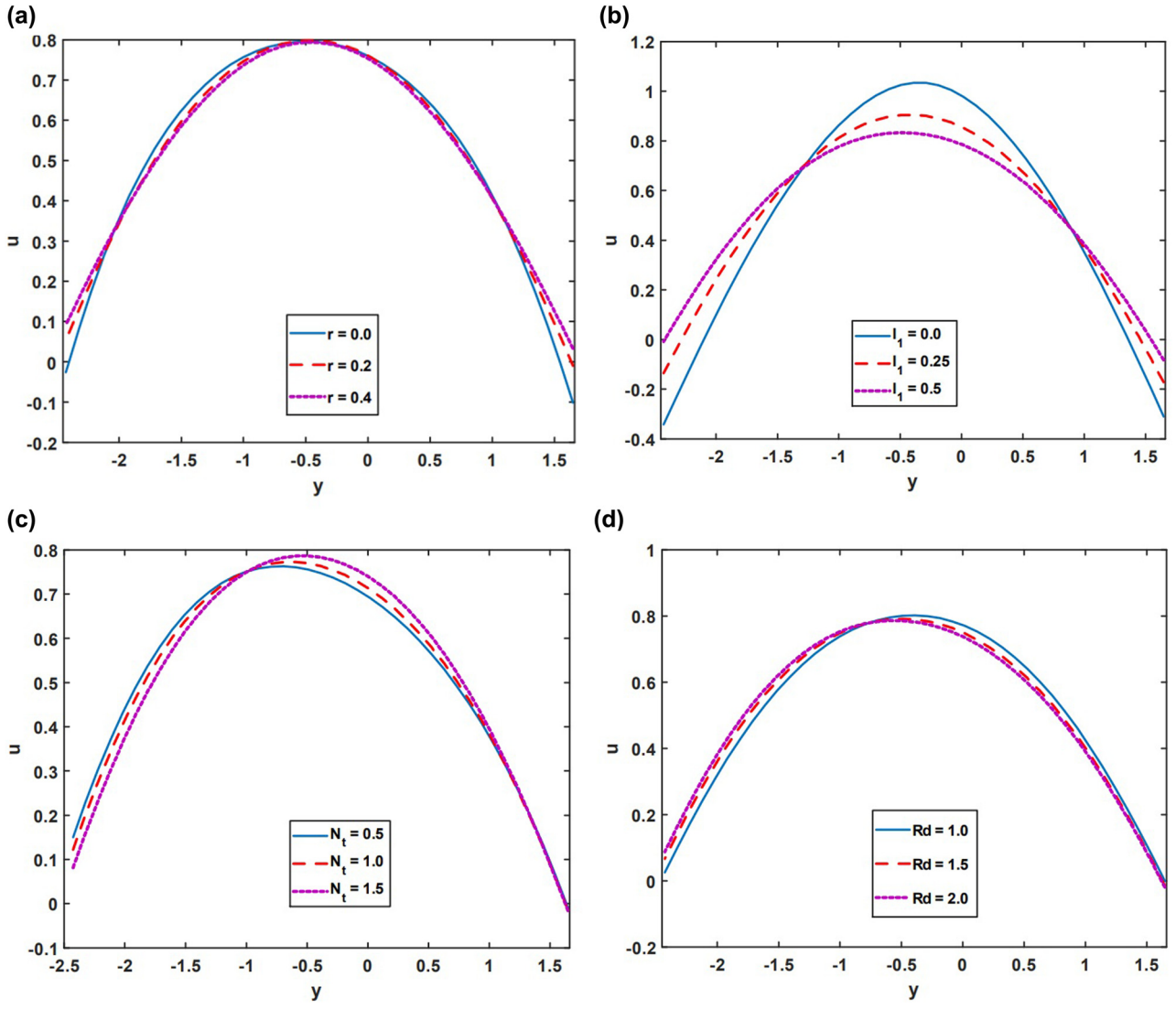

Figure 4: Behaviour of velocity profile on r, l_1, N_t and Rd.

The effects of pressure rise on non-Newtonian parameter (r), velocity slip (l_1), thermophoresis parameter (N_t), and thermal slip (l_2) are analysed in Figure 2(a)–(c). To expose all aspects of pressure rise, the pumping phases are classified into the following segments:

a) The augmented region exists when $Q < 0$ and $\Delta p < 0$: The pressure induced by the peristaltic force enhances flow in this area.
b) The peristaltic region exists when $Q > 0$ and $\Delta p > 0$ gt is 0: Fluid is propelled in the direction of flow by peristalsis waves, which continually regulates the pressure in this area.
c) The retrograde region exists when $Q < 0$ and $\Delta p > 0$: Peristalsis contractions are preventing the flow in this area, which increase pressure in the direction opposite to the flow. The retrograde motion may generate a "backflow" effect that spreads the fluid and avoids system congestion.
d) The free pumping region exist when $\Delta p = 0$ and $Q = 0$: Peristalsis walls are the sole means of flow in this region.

It is seen from Figure 2(a) that increasing the influence of the non-Newtonian parameter (r) increases the pressure rise in the zones of retrograde, free, and peristaltic pumping, but the reverse effect is seen in the augmented region. Here pressure rise drops because of the rising influence of r. In Figure 2(b), it is shown that as the influence of velocity slip (l_1) increases, the pressure rise falls in the peristaltic, free, and retrograde pumping zones, but the opposite behaviour is noted in the augmented pumping region. The rising influence of velocity slip causes pressure to increase in this

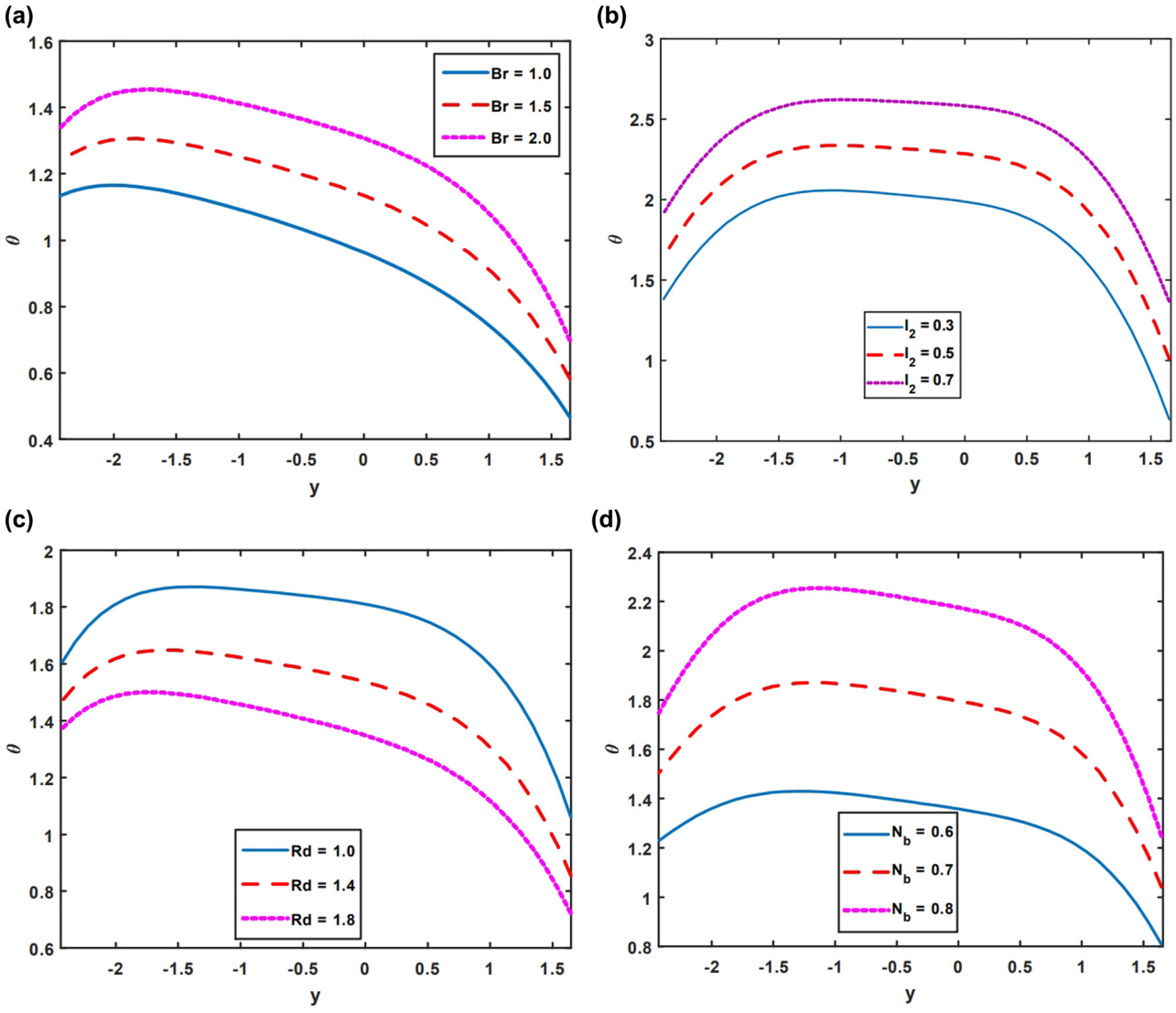

Figure 5: Behaviour of temperature profile on impact on Br, l_2, Rd and N_b .

region. As observed in Figure 2(c) and (d), increasing the thermophoresis (N_t) and thermal slip (l_2) parameters cause pressure to increase in all peristaltic pumping zones. Figure 3(a)–(d) depicts the significance of various parameters on the pressure gradient distribution. It is noted from Figure 3(a) that increasing the non-Newtonian variable causes the pressure gradient to accelerate at the central region of the channel while decreasing towards the right and left sides. According to Figure 3(b), the pressure gradient reduces in the region $x \in [0.3,0.6]$ due to the increasing impact of velocity slip, whereas it increases in the regions $x \in [0,0.3]$ and $x \in [0.6,1]$. As illustrated in Figure 3(c) and (d), the pressure gradient drops as a result of the increasing impact of nanoparticle Grashof number (G_{rF}) and thermal radiation (Rd).

The phenomenon of flow velocity is investigated in Figure 4(a)–(d) for various values of non-Newtonian parameter (r), velocity slip (l_1), thermophoresis (N_t), and thermal radiation (Rd). As depicted in Figure 4(a), when the fluid is in the range $x \in [-2.45, -2]$ and $x \in [1,1.6]$, the velocity of the fluid rises owing to the increase in the influence of the non-Newtonian parameter, but when the fluid is at the channel's centre at $x = -0.5$, the maximum fluid velocity exists. Furthermore, as fluid approaches the regions $x \in [-2.0, -0.6]$ and $x \in [-0.6,1.0]$, the velocity begins to decrease due to the increasing behaviour of r. According to Figure 4(b), the velocity of fluid drops in the region $x \in [-1.3,0.8]$ as the effect of velocity slip parameter (l_1) increases. Furthermore, similar behaviour of fluid velocity is noted in the regions $x \in [-2.45, -1.3]$ and $x \in [0.8,1.6]$.

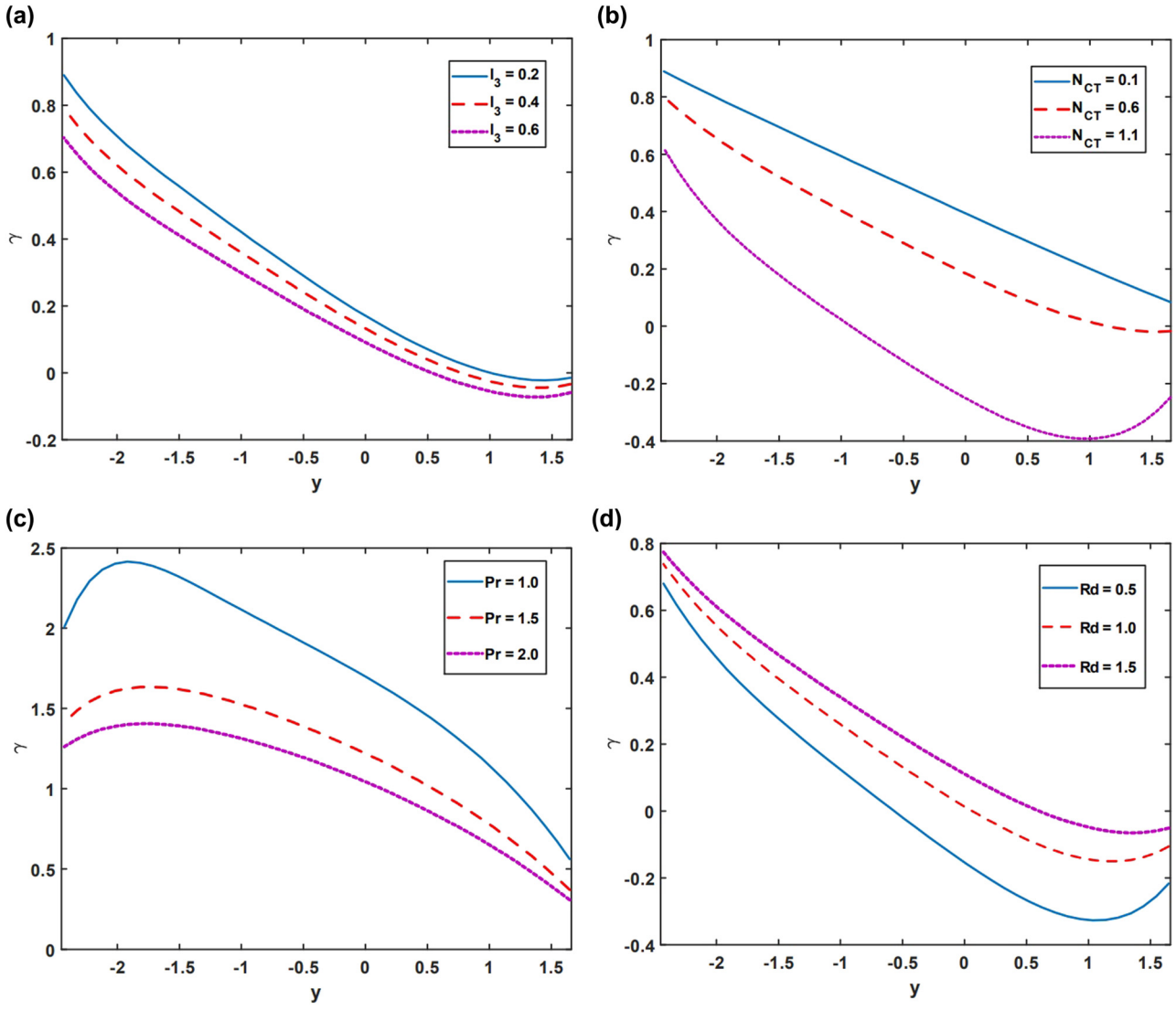

Figure 6: Behaviour of solutal concentration impact on l_3, N_{CT}, Pr, and Rd.

Here magnitude value of fluid velocity decreases as l_1 increases. As shown in Figure 4(c), fluid velocity tends to rise when it is in the region $x \in [-1.0,1.6]$, but it tends to drop when it is in the region $x \in [-2.5, -1]$ due to an increase in the influence of thermophoresis (N_t) parameter. The fluid velocity exhibits opposite behaviour on thermal radiation (Rd) when compared to the thermophoresis (N_t) parameter. The velocity profile enhances when fluid is in the region $x \in [-2.5, -1.3]$ and drops when the fluid is in the region $x \in [-1.3,1.6]$ due to the enhancing influence of thermal radiation (Figure 4(d)).

Figure 5(a)–(d) displays the effect of temperature distribution on Brinkman number (Br), thermal slip parameter (l_2), radiation parameter (Rd), and Brownian motion (N_b). Figure 5(a) illustrates the impact of Brinkman number (Br) on temperature distribution. It is demonstrated in this figure that by using Br, it is possible to increase the internal resistance among the fluid's particles, which leads to a better temperature distribution. A similar characteristic is being investigated in Figure 5(b) for the thermal slip parameter (l_2). Figure 5(c) shows the graphical impact of temperature on radiation (Rd) parameter. This figure illustrates that increasing the values of the radiation parameter reduces temperature. It is due to the fact that as the radiation parameter rises, heat conduction is reduced, and electromagnetic wave motion is improved. Because irregular atom growth leads to dispersion of heat exchange, when it is sent out, the adjoining particles spread less and the vitality exchange rate between them slows down. Diffusive heat exchange also happens more slowly than radiative heat exchange. It is noted in Figure 5(d) that the system's temperature may change as a result of the

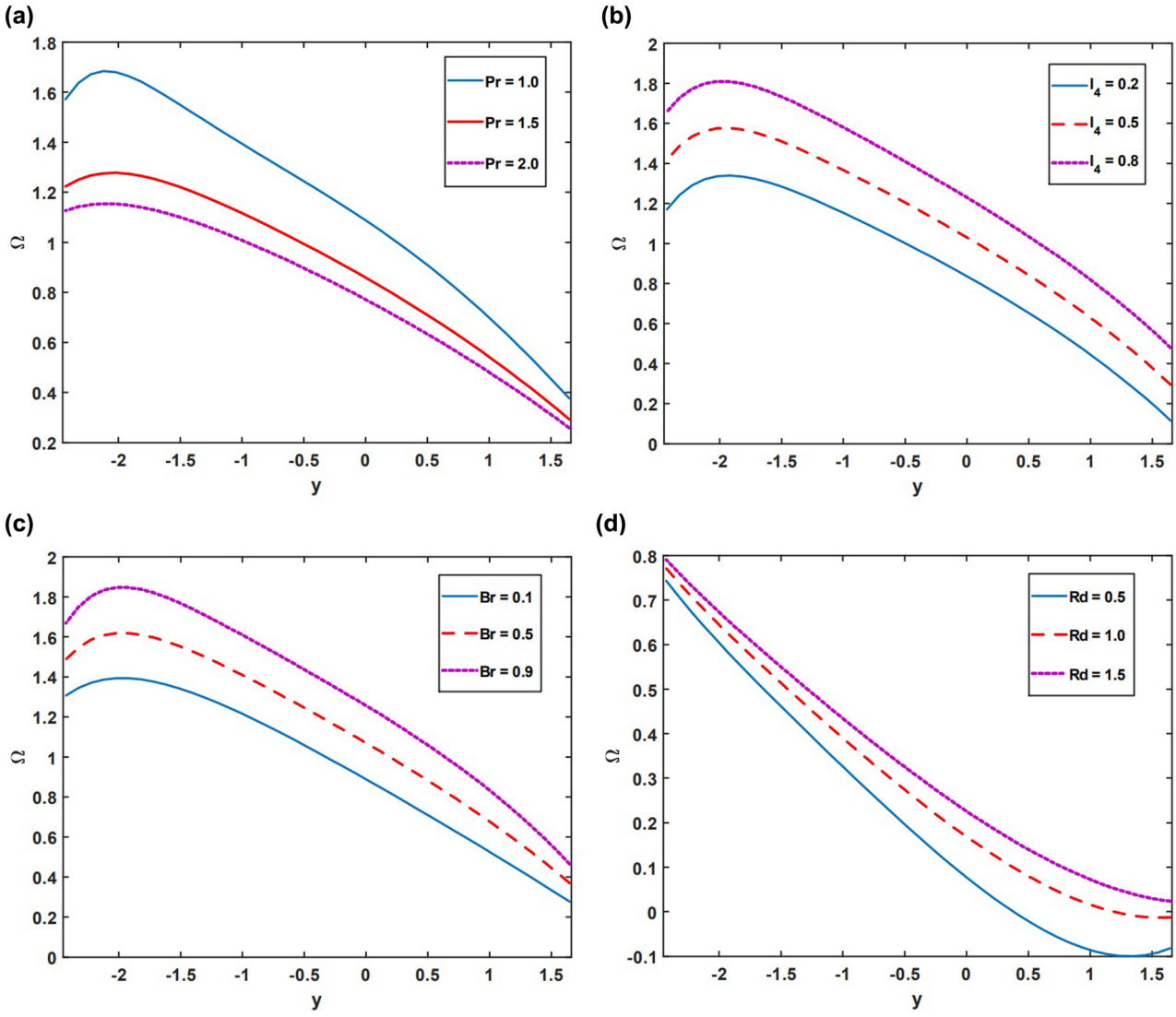

Figure 7: Behaviour of nanoparticle volume fraction on Pr, l_4, Br, and Rd.

enhanced Brownian motion. This occurs because when particles collide more frequently and violently, some of their kinetic energy is transferred to the suspended particles. The particles internal energy is increased, and their temperature is raised as a result of the energy transfer. Therefore, a rise in Brownian motion usually correlates with a rise in temperature.

Figure 6(a)–(d) displays the characteristics of solutal concentration on slip parameter of concentration (l_3), Soret parameter (N_{CT}), Prandtl number (Pr), and radiation parameter (Rd). Figure 6(a) demonstrates that the concentration profile decreases as a result of the increasing influence of the concentration's slip parameter (l_3). It is noted in Figure 6(b) that due to the increasing impact of the Soret parameter, the profile of concentration tends to drop. The Soret parameter shows a higher impact of heat diffusion on concentration profiles as it rises. In these situations, the concentration profile frequently exhibits a tendency to decline or become more reduced in areas of greater temperature. As seen in Figure 6(c), a rise in the Prandtl number causes irregularities and a general drop in the particle distribution. The flow field's temperature rise is the primary factor in the lowering of nanoparticle concentration, which is caused by the temperature of the channel. The radiation parameter exhibits opposite effect on concentration profile when compared to l_3, N_{CT}, and Pr. The concentration profile rises due to the increasing influence of heat radiation. Increased movement of molecules and energy transfer throughout the system might be a result of high radiation intensity. This improved molecular mobility may cause diffusion coefficients to rise, facilitating the transport of particles throughout the medium. The

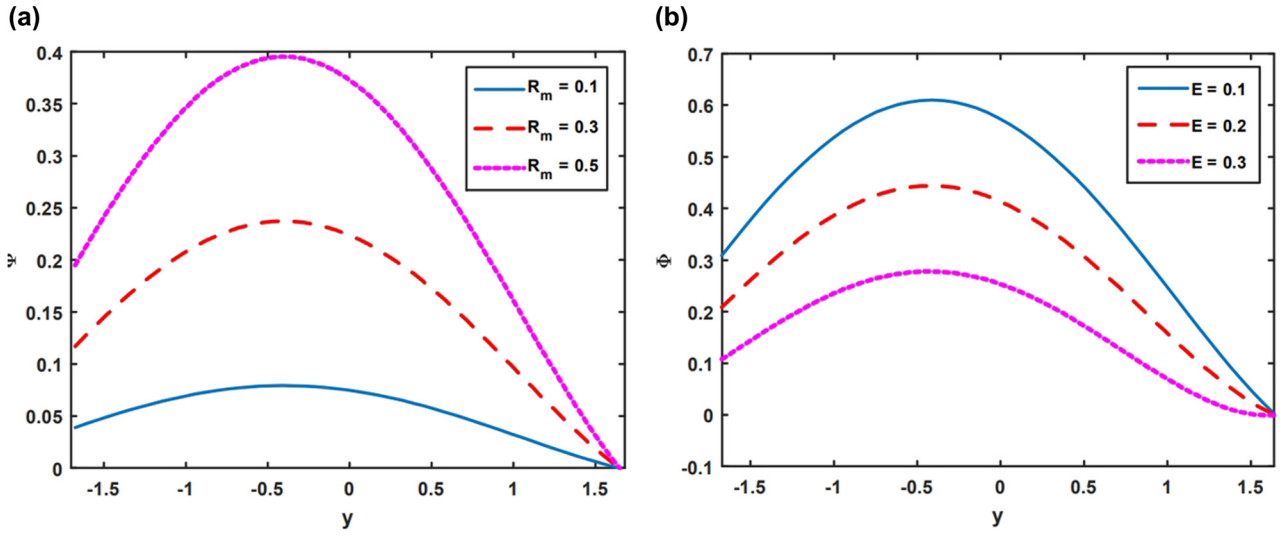

Figure 8: Behaviour of magnetic force function on R_m and E.

concentration profile may consequently stretch out or become more diffuse, increasing concentration across a larger region, as seen in Figure 6(d).

Figure 7(a)–(d) shows how the nanoparticles volume fraction affects several fluid properties such as Prandtl number (Pr), nanoparticle slip parameter (l_4), Brinkman number (Br), and thermal radiation (Rd). The graph in Figure 7(a) demonstrates the effect of nanoparticle volume fraction on Prandtl number (Pr). Figure 7(a) illustrates that when the effect of the Prandtl number increases, the nanoparticle volume fraction profile decreases. From Figure 7(b), it is seen that the profile of nanoparticle volume fraction enhances when the impact of nanoparticle slip parameter increases. It is highlighted in Figure 7(c) that when the Brinkman number increases, the convective flow dominates. The fluid's nanoparticles may mix more effectively as a result of the enhanced flow. The outcome is a greater nanoparticle volume percentage because the nanoparticles are spread more uniformly. It is observed from Figure 7(d) that increasing the radiation parameter may result in considerable fluid heating or temperature gradients. As a result, thermal buoyancy forces may be produced, causing convective fluid motion. Increased convection promotes nanoparticle dispersion and mixing throughout the fluid resulting in a higher nanoparticle volume fraction.

Figure 8(a) and (b) show the effects of the magnetic force function on the magnetic Reynolds number (R_m) and electric field (E). To study the impact of magnetic force function on magnetic Reynolds number (R_m) and electric field (E) , Figure 8(a) and (b) are plotted. As seen in Figure 8(a), the magnetic force function frequently increases as the magnetic Reynolds number increases, indicating that magnetic induction impact on fluid behaviour is becoming more important. The profile of magnetic force function decreases when the intensity of electric field increases (Figure 8(b)).

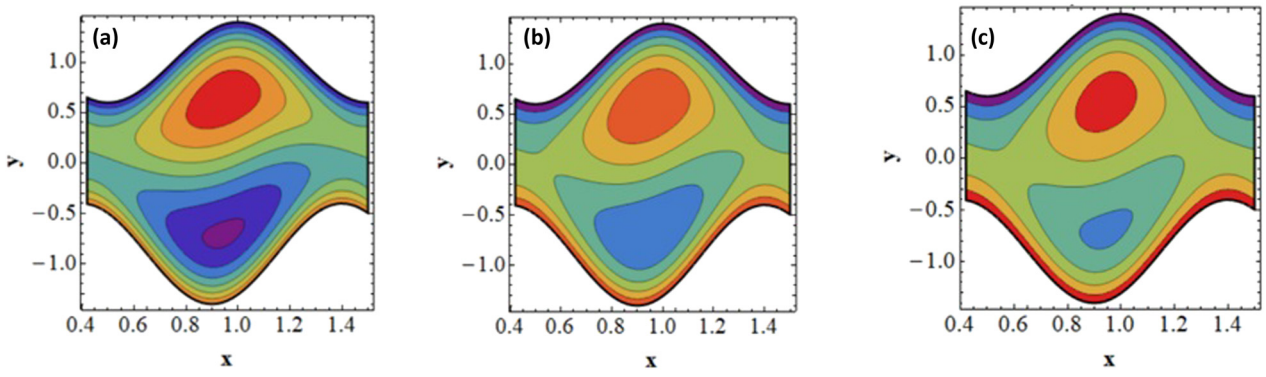

Figure 9: Impact of velocity slip parameter (l_1) on streamlines. (a) l_1 = 0.0; (b) l_1 = 0.1 and (c) l_1 = 0.2.

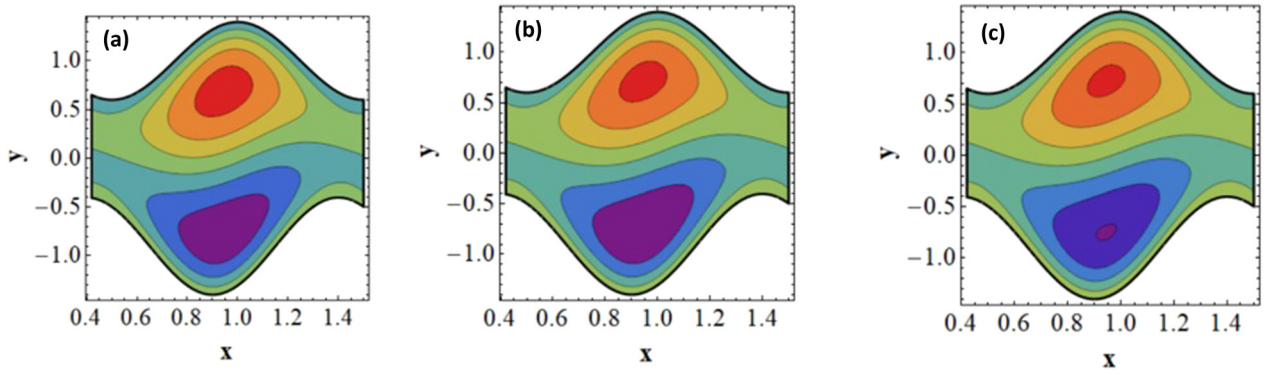

Figure 10: Impact of thermal slip parameter (l_2) on streamlines. (a) l_2 = 0.0; (b) l_2 = 0.4 and (c) l_2 = 0.8.

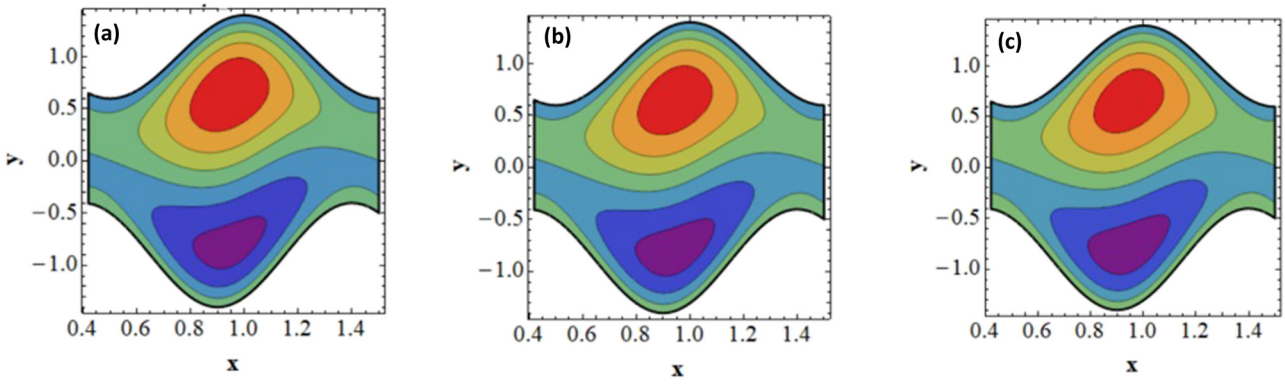

Figure 11: Impact of concentration slip parameter (l_3) on streamlines. (a) l_3 = 0.0; (b) l_3 = 0.2 and (c) l_3 = 0.4.

4.1 Streamlines

The conceptual lines, used in fluid dynamics, are called streamlines. These hypothetical lines depict the instantaneous direction of fluid movement at varying points within the fluid field. When taken into consideration in the study of peristaltic flow, the streamlines have significance as they provide valuable insights through flow patterns and pathways of fluid particles in the system. Hence, the streamlines analysis is beneficial for the development and enhancement of peristaltic flow system. The visualization of streamlines enables the researchers to detect zones of flow separation areas, characterized by elevated sheer stress, or potential sites for particle deposition. This

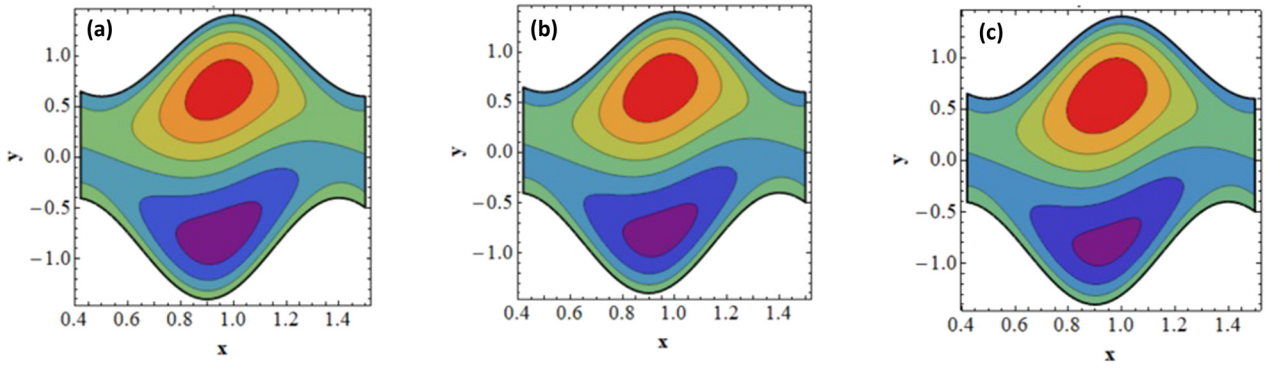

Figure 12: Impact of nanoparticle slip parameter (l_4) on streamlines. (a) l_4 = 0.0; (b) l_4 = 0.4 and (c) l_4 = 0.8.

knowledge is invaluable as it can be used to develop more efficient peristaltic devices or improve the parameters matrix for specified flow characteristics.

The impact of streamlines on velocity slip (l_1), thermal slip (l_2), concentration slip (l_3), and nanoparticle slip (l_4) parameters are examined in Figures 9–12. According to Figure 9, the quantity and shape of the trapped bolus reduces in both the top and bottom regions of the channel as the velocity slip increases. This occurs because velocity slip may strengthen the fluid mixing, especially at channel boundaries. This improved mixing may have an impact on the bolus' solute or particle distribution, which may change the bolus' composition and characteristics. As shown in Figure 10, the appearance of the trapped bolus changes in the top area of the channel as the influence of the thermal slip parameter increases, whereas the number of trapped boluses increases in the bottom region. In Figure 11, it is shown that when the concentration slip parameter increases, the size of the trapped bolus decreases in the top region of the channel while increasing in the bottom. The opposite behaviour is noted when nanoparticle parameter increases. According to Figure 12, the volume of the trapped bolus increases due to the increasing impact of nanoparticle slip parameter, whereas in the lower part, the trapped bolus decreases.

5 Conclusion

The study looks at the phenomena of double-diffusive convection making use of the Sisko nanofluid model. It illustrates the effects of induced magnetic field, viscous dissipation, and heat radiation in an asymmetric geometry with numerous slip conditions. The convective double diffusion phenomena are described by the Soret and Dufour parameters. Mathematical formulation of the proposed model is carried out in 2-dimensional and 2-directional flow. A group of nonlinear partial differential equations are generated by the mathematical modelling of fluid flow. Using Mathematica's built-in NDSolve program, the coupled nonlinear differential equations are numerically computed. Graphical data are shown to highlight the importance of various physiological features of flow amounts. The following are the key conclusions drawn from this investigation:

- As the radiation parameter increases, the distribution of temperature decreases as a result of the system's significant heat radiation and thereby resulting in cooling effects.
- An increase in the Brownian motion corresponds to an increase in the temperature distribution because when particles collide more frequently and strongly, some of their kinetic energy is transmitted to the suspended particles. As a result of the energy transfer, the particles' internal energy increases and their temperature rises.
- Heat diffusion has a greater effect on the concentration profile as the Soret parameter increases.
- An increasing impact of heat radiation causes the concentration profile to increase.
- The nanoparticle volume fraction profile lessens as the Prandtl number's influence increases.
- When a fluid's temperature changes due to thermal radiation, buoyancy effects occur that cause the fluid to rise to a higher level, which can increase the volume fraction of nanoparticles.
- As the velocity slip rises, the trapped bolus shape and size are reduced in both the upper and bottom parts of the channel.
- The volume of the confined bolus reduces in the upper part of the channel while boosting in the bottom as the concentration slip parameter rises.

Acknowledgments: This work was supported by the Deanship of Scientific Research, Vice Presidency for Graduate Studies and Scientific Research, King Faisal University, Saudi Arabia (Grant No. 6012).

Funding information: This work was supported by the Deanship of Scientific Research, Vice Presidency for Graduate Studies and Scientific Research, King Faisal University, Saudi Arabia (Grant No. 6012).

Author contributions: H.Y., S.A., M.A., and A.R.: developed the mathematical modelling for the proposed problem, suggested the solution for the problem, written the manuscript, and supervised the project; H.Y., K.S., J.G.A.: provided graphical conclusions, mathematical simulation of the proposed problem, solved the problem, and revised the manuscript; S. A., A. R., K.S., J.G.A.: examined the theory validation and drawn the graphical conclusion. H.Y.: provided funding. All authors have accepted responsibility for the entire content of this manuscript and approved its submission.

Conflict of interest: The authors state no conflict of interest.

References

[1] Latham TW. Fluid motion in a peristaltic pump, M.Sc. Thesis. Cambridge: MIT; 1966.

[2] Shapiro AH, Jaffrin MY, Weinberg SL. Peristaltic pumping with long wavelengths at low Reynolds number. Cambridge Univ Press. 1969;37:799–825.
[3] Mishra M, Rao AR. Peristaltic transport of a Newtonian fluid in an asymmetric channel. Z Angew Math Phys. 2003;54:532–50.
[4] Hina S, Hayat T, Asghar S. Peristaltic transport of Johnson-Segalman fluid in a curved channel with wall compliant properties. Nonlinear Anal: Model Control. 2012;17:297–311.
[5] Akbar NS, Hayat T, Nadeem S, Obaidat S. Peristaltic flow of a Williamson fluid in an inclined asymmetric channel with partial slip and heat transfer. Int J Heat Mass Transf. 2012;55:1855–62.
[6] Safia Akram KHS, Mekheimer S. Nadeem, Influence of lateral walls on peristaltic flow of a couple stress fluid in a non-uniform rectangular duct. Appl Maths Inf Sci. 2014;8:1127–33.
[7] Nadeem S, Akbar NS. Peristaltic flow of Sisko fluid in a uniform inclined tube. Acta Mech Sin. 2010;26:675–83.
[8] Nadeem S, Akhtar S, Saleem A, Akkurt N, Almutairi S, Ghazwani HA, Eldin SM. Entropy analysis for a novel peristaltic flow in a curved heated endoscope: an application of applied sciences. Sci Rep. 2023;13:1504.
[9] Nadeem S, Akram S. Peristaltic transport of a hyperbolic tangent fluid model in an asymmetric channel. Z Naturforsch A. 2009;64:559–67.
[10] Nadeem S, Akram S. Peristaltic flow of a Williamson fluid in an asymmetric channel. Commun Nonlinear Sci Numer Simul. 2010;15:1705–16.
[11] Choi SUS, Eastman JA. Enhancing thermal conductivity of fluids with nanoparticles. In Proceedings of Enhancing Thermal Conductivity of Fluids with Nanoparticles. 231, San Francisco, CA, USA: American Society of Mechanical EngineersFED; 1995. p. 99–105 New York, NY, USA.
[12] Masuda H, Ebata A, Teramae K. Alteration of thermal conductivity and viscosity of liquids by dispersing ultra-fine particles. Netsu Bussei. 1993;7:227–33.
[13] Daungthongsuk W, Wongwises S. Effect of thermophysical properties models on the predicting of the convective heat transfer coefficient for low concentration nanofluid. Int Commun Heat Mass Transf. 2008;35:1320–6.
[14] Buongiorno J, Hu W. Nanofluid coolants for advanced nuclear power plants, (ICAPP'05). Seoul, Korea: May 2005.
[15] Buongiorno J. Convective transport in nanofluids. J Heat Transf. 2005;128:240–50.
[16] Mani A, Zangle TA, Santiago JG. On the propagation of concentration polarization from microchannel-nanochannel interfaces part I: analytical model and characteristic analysis. Langmuir. 2009;25:3898–908.
[17] Akbar NS, Nadeem S. Endoscopic effects on peristaltic flow of a nanofluid. Commun Theor Phys. 2011;56:761–8.
[18] Akbar NS. Peristaltic Sisko nanofluid in an asymmetric channel. Appl Nanosci. 2014;4:663–73.
[19] Tripathi D, Bég OA. A study on peristaltic flow of nanofluids: Application in drug delivery systems. Int J Heat Mass Transf. 2014;70:61–70.
[20] Ramzan M, Bilal M, Chungy JD. Radiative Williamson nanofluid flow over a convectively heated Riga plate with chemical reaction-A numerical approach. Chin J Phys. 2017;55:1663–73.
[21] Bilal M, Ramzan M, Siddique I, Sajjad A. Magneto-micropolar nanofluid flow through the convective permeable channel using Koo–Kleinstreuer–Li model. J Magn Magn Mater. 2023;565:170288.
[22] Aly EH, Ebaid A. Exact analytical solution for the peristaltic flow of nanofluids in an asymmetric channel with slip effect of the velocity, temperature and concentration. J Mech. 2014;30:411–22.
[23] Nadeem S, Riaz A, Ellahi R, Akbar NS. Mathematical model for the peristaltic flow of nanofluid through eccentric tubes comprising porous medium. Appl Nanosci. 2014;4:733–43.
[24] Alhowaity A, Mehmood Y, Hamam H, Bilal M. Radiative flow of nanofluid past a convected vertical Riga plate with activation energy and nonlinear heat generation. Proc Inst Mech Eng, Part E: J Process Mech Eng. 2023;237(5):1799–807.
[25] Bilal M, Ramzan M, Zafar R, Siddique I. A finite thin film flow of pseudo-plastic MHD hybrid nanofluid with heat generation and variable thermal conductivity. Waves Random Complex Media. 2023. doi: 10.1080/17455030.2023.2177502.
[26] Hayat T, Tanveer A, Alsaedi A. Numerical analysis of partial slip-on peristalsis of MHD Jeffery nanofluid in curved channel with porous space. J Mol Liq. 2016;224:944–53.
[27] Mekheimer KS, Hasona WM, Abo-Elkhair RE, Zaher AZ. Peristaltic blood flow with gold nanoparticles as a third grade nanofluid in catheter: Application of cancer therapy. Phys Lett A. 2018;382:85–93.
[28] Ellahi R, Sait SM, Shehzad N, Mobin N. Numerical simulation and mathematical modeling of electro-osmotic Couette–Poiseuille flow of MHD power-law nanofluid with entropy generation. Symmetry. 2019;11:1038.
[29] Bhatti MM, Zeeshan A, Ellahi R. Simultaneous effects of coagulation and variable magnetic field on peristaltically induced motion of Jeffrey nanofluid containing gyrotactic microorganism. Microvasc Res. 2017;110:32–42.
[30] Hayat T, Farooq S, Ahmad B, Alsaedi A. Homogeneous-heterogeneous reactions and heat source/sink effects in MHD peristaltic flow of micropolar fluid with Newtonian heating in a curved channel. J Mol Liq. 2016;223:469–88.
[31] Shit GC, Roy M, Eddie YK. Ng, Effect of induced magnetic field on Peristaltic flow of a micropolar fluid in an asymmetric channel. Int J Numer Methods Biomed Eng. 2010;26:1380–403.
[32] Shit GC, Ranjit NK, Sinha A, Roy M. Effect of induced magnetic field on peristaltic transport of a micropolar fluid in the presence of slip velocity. Int J Appl Maths Mech. 2014;10:81–107.
[33] Akram S, Nadeem S, Hanif M. Numerical and analytical treatment on peristaltic flow of Williamson fluid in the occurrence of induced magnetic field. J Magn Magn Mater. 2013;346:142–51.
[34] Akram S, Nadeem S. Influence of induced magnetic field and heat transfer on the peristaltic motion of a Jeffrey fluid in an asymmetric channel: closed form solutions. J Magn Magn Mater. 2013;328:11–20.
[35] Reddy MG, Makinde OD. Magnetohydrodynamic peristaltic transport of Jeffrey nanofluid in an asymmetric channel. J Mol Liq. 2016;223:1242–8.
[36] Bhatti MM, Sheikholeslami M, Zeeshan A. Entropy analysis on electro-kinetically modulated peristaltic propulsion of magnetized nanofluid flow through a microchannel. Entropy. 2017;19:481.
[37] Bhatti MM, Zeeshan A. Study of variable magnetic field and endoscope on peristaltic blood flow of particle-fluid suspension through an annulus. Biomed Eng Lett. 2016;6:242–9.
[38] Akbar NS, Tripathi D, Khan ZH, Bég OA. Mathematical model for ciliary induced transport in MHD flow of Cu/H_2O nanofluids with magnetic induction. Chin J Phys. 2017;55:947–62.

[39] Safia Akram SN. Consequence of nanofluid on peristaltic transport of a hyperbolic tangent fluid model in the occurrence of apt (tending) magnetic field. J Magn Magn Mater. 2014;358:183–91.
[40] Hayat T, Bilal Ahmed FM, Abbasi AA. Numerical investigation for peristaltic flow of Carreau-Yasuda magneto-nanofluid with modified Darcy and radiation. J Therm Anal Calorim. 2019;137:1359–67.
[41] Sadia Ayub T, Hayat S, Asghar B. Ahmad, Thermal radiation impact in mixed convective peristaltic flow of third grade nanofluid. Results Phys. 2017;7:3687–95.
[42] Hussain Q, Latif T, Alvi N, Asghar S. Nonlinear radiative peristaltic flow of hydromagnetic fluid through porous medium. Results Phys. 2018;9:121–34.
[43] Kothandapani M, Prakash J. Effects of thermal radiation parameter and magnetic field on the peristaltic motion of Williamson nanofluids in a tapered asymmetric channel. Int J Heat Mass Transf. 2015;81:234–45.
[44] Hayat T, Nisar Z, Yasmin H, Alsaedi A. Peristaltic transport of nanofluid in a compliant wall channel with convective conditions and thermal radiation. J Mol Liq. 2016;220:448–53.
[45] Mojtabi A, Charrier-Mojtabi MC. Double diffusive convection in porous media. In: Vafai K, editor. Handbook of Porous Media. New York, NY, USA: Taylor and Francis; 2005. p. 269–320.
[46] Ostrach S. Natural convection with combined driving forces. Physicochem Hydrodyn. 1980;1:233–47.
[47] Sharma A, Tripathi D, Sharma RK, Tiwari AK. Analysis of double diffusive convection in electroosmosis regulated peristaltic transport of nanofluids. Phys A: Stat Mech Appl. 2019;535:122148.
[48] Akram S, Afzal Q, Aly EH. Half-breed effects of thermal and concentration convection of peristaltic pseudoplastic nanofluid in a tapered channel with induced magnetic field. Case Stud Therm Eng. 2020;22:100775.
[49] Asha SK, Sunitha G. Influence of thermal radiation on peristaltic blood flow of a Jeffrey fluid with double diffusion in the presence of gold nanoparticles. Inform Med Unlocked. 2019;17:100272.
[50] Anwar Bég O, Tripathi D. Mathematica simulation of peristaltic pumping with double-diffusive convection in nanofluids: a bio-nanoengineering model. Proc Inst Mech Eng, Part N: J Nanoeng Nanosyst. 2012;225:99–114.
[51] Alolaiyan H, Riaz A, Razaq A, Saleem N, Zeeshan A, Bhatti MM. Effects of double diffusion convection on third grade nanofluid through a curved compliant peristaltic channel. Coatings. 2020;10(2):154.
[52] Akram S, Athar M, Saeed K, Razia A. Influence of an induced magnetic field on double diffusion convection for peristaltic flow of thermally radiative Prandtl nanofluid in non-uniform channel. Tribol Int. 2023;187:108719.
[53] Asha SK, Sunitha G. Thermal radiation and Hall effects on peristaltic blood flow with double diffusion in the presence of nanoparticles. Case Stud Therm Eng. 2020;17:100560.
[54] Riaz A, Nadeem S, Ellahi R, Zeeshan A. Exact solution for peristaltic flow of Jeffrey fluid model in a three-dimensional rectangular duct having slip at the walls. Appl Bionics Biomech. 2014;11:81–90.
[55] Mehmood OU, Mustapha N, Shafie S, Fetecau C. Simultaneous effects of dissipative heating and partial slip-on peristaltic transport of Sisko fluid in asymmetric channel. Int J Appl Mech. 2014;6:1450008.
[56] Mandviwalla X, Archer R. The influence of slip boundary conditions on peristaltic pumping in a rectangular channel. J Fluids Eng. 2008;130:124501.
[57] Khan Y, Athar M, Akram S, Saeed K, Razia A, Alameer A. Roll of partial slip-on Ellis nanofluid in the proximity of double diffusion convection and tilted magnetic field: Application of Chyme movement. Heliyon. 2023;9:e14760.
[58] Akram S, Mekheimer K, Elmaboud YA. Particulate suspension slip flow induced by peristaltic waves in a rectangular duct: Effect of lateral walls. Alex Eng J. 2018;57:407–14.
[59] saeed K, akram S, ahmad A. Outcomes of partial slip-on double-diffusive convection on peristaltic waves of Johnson–Segalman nanofluids under the impact of inclined magnetic field. Arab J Sci Eng. 2023;48:15865–81. doi: 10.1007/s13369-023-07706-y.